

## THE ABUNDANCE OF INTERSTELLAR BORON<sup>1</sup>

J. CHRISTOPHER HOWK,<sup>2</sup> KENNETH R. SEMBACH,<sup>2</sup> AND BLAIR D. SAVAGE<sup>3</sup>

Received 2000 May 23; accepted 2000 June 1

### ABSTRACT

We use new Space Telescope Imaging Spectrograph (STIS) and archival Goddard High Resolution Spectrograph (GHRS) observations to study interstellar B II  $\lambda$ 1362 and O I  $\lambda$ 1355 absorption along seven sight lines. Our new column density measurements, combined with measurements of four sight lines from the literature, allow us to study the relative B/O abundances over a wide range of interstellar environments. We measure sight-line-integrated relative gas-phase abundances in the range  $[B/O] = -1.00$  to  $-0.17$ , and our data show that the B/O abundances are anticorrelated with average sight line densities over the range  $\log \langle n_H \rangle \approx -1.3$  to  $+0.7$ . Detailed comparisons of the B II and O I line shapes show that the B/O ratio is significantly higher in warm interstellar clouds than in cool clouds. These results are consistent with the incorporation of boron into dust grains in the diffuse ISM. Since boron is likely incorporated into grains, we derive a lower limit to the present-day total (gas + dust) interstellar boron abundance of  $B/H \gtrsim (2.5 \pm 0.9) \times 10^{-10}$ . The effects of dust depletion and ionization differences from element to element will make it very difficult to reliably determine  $^{11}B/^{10}B$  along most interstellar sight lines.

*Subject headings:* ISM: abundances — ISM: atoms — ultraviolet: ISM

### 1. INTRODUCTION

Production of the light element boron in standard big bang nucleosynthesis models is negligible (see, e.g., Pagel 1997). The chemical evolution of boron is determined by its production through cosmic-ray spallation of interstellar material (Reeves, Fowler, & Hoyle 1970; Meneguzzi, Audouze, & Reeves 1971) and/or neutrino-induced spallation in Type II supernovae (Woodsley et al. 1990) and its destruction via astration. The evolution of the cosmic boron abundance therefore reflects the cosmic-ray flux and/or supernova rate history in the Milky Way. Measurements of stellar boron abundances have revealed a trend of increasing B/H over time (as expected), from  $B/H \sim 2 \times 10^{-12}$  in very metal poor halo stars (Edvardsson et al. 1994; Duncan et al. 1997) to the much higher Orion association [ $B/H \approx (3-6) \times 10^{-10}$ ; Cunha et al. 1997] and solar system (meteoritic) abundances [ $B/H = (7.6 \pm 0.7) \times 10^{-10}$ ; Anders & Grevesse 1989]. Because there is evidence that the solar system may be enhanced in metals such as oxygen relative to the local interstellar medium (ISM; e.g., Meyer, Jura, & Cardelli 1998), young B stars (e.g., Gies & Lambert 1992; Kilian-Montenbruck, Gehren, & Nissen 1994), and H II regions (e.g., Peimbert, Torres-Peimbert, & Dufour 1993), it is unclear that the solar system B/H is the best fiducial point for the present-day boron abundance in studies of Galactic chemical evolution. The boron abundance of the present-day ISM may be more appropriate for such studies. The differences between the solar system and the ISM could yield important information on the recent chemical evolution of the solar neighborhood.

<sup>1</sup> Based on observations made with the NASA/ESA *Hubble Space Telescope*, obtained from the data archive at the Space Telescope Science Institute. STScI is operated by the Association of Universities for Research in Astronomy, Inc. under NASA contract NAS 5-26555.

<sup>2</sup> Department of Physics and Astronomy, The Johns Hopkins University, Baltimore, MD 21218; howk@pha.jhu.edu, sembach@pha.jhu.edu.

<sup>3</sup> Department of Astronomy, University of Wisconsin–Madison, Madison, WI 53706; savage@astro.wisc.edu.

Here we present new high-resolution observations of interstellar B II  $\lambda$ 1362.461 and O I  $\lambda$ 1355.598 absorption toward the stars HD 104705, HD 121968, HD 177989, HD 218915, and HD 303308 taken with STIS on board the *Hubble Space Telescope* (HST). We also present analyses of the B/O abundances along the  $\alpha$  Sco B and  $\zeta$  Oph sight lines using archival GHRS data sets. We have more than doubled the measurements of interstellar boron, and the available data now probe a wide range of diffuse ISM environments. After discussing our observations in § 2, we will show in § 3 that the present-day interstellar B/H ratio seems to be dominated by the incorporation of boron into dust grains. Thus, the interstellar gas-phase boron abundance provides only a lower limit to the total (gas + dust) interstellar boron abundance.

### 2. OBSERVATIONS AND REDUCTIONS

The STIS data used here were obtained as part of our STIS GO program (number 7270), with the exception of the HD 303308 data, which were obtained from the STIS archive. In all cases the observations employed the far-ultraviolet MAMA detector and the E140H grating with the light from the star passing through the  $0''.2 \times 0''.09$  aperture. The resolution of these data is  $\Delta v \sim 2.7 \text{ km s}^{-1}$  (FWHM). The data were extracted and the backgrounds estimated as described by Howk & Sembach (2000). For spectral regions covered in multiple orders (or observations), we have coadded the flux-calibrated data and weighted the contribution of each individual spectrum by the inverse square of its error vector.

The archival, post-COSTAR GHRS data used in this work were reduced as discussed by Howk, Savage, & Fabian (1999). The  $\alpha$  Sco B data were obtained through the large science aperture, while the  $\zeta$  Oph data were obtained through the small science aperture. Both data sets employed the Ech-A grating, yielding a resolution of  $\Delta v \sim 3.5 \text{ km s}^{-1}$  (FWHM).

Figure 1 shows the STIS spectra, and Table 1 gives the measured equivalent widths,  $W_\lambda$ , for the new STIS and

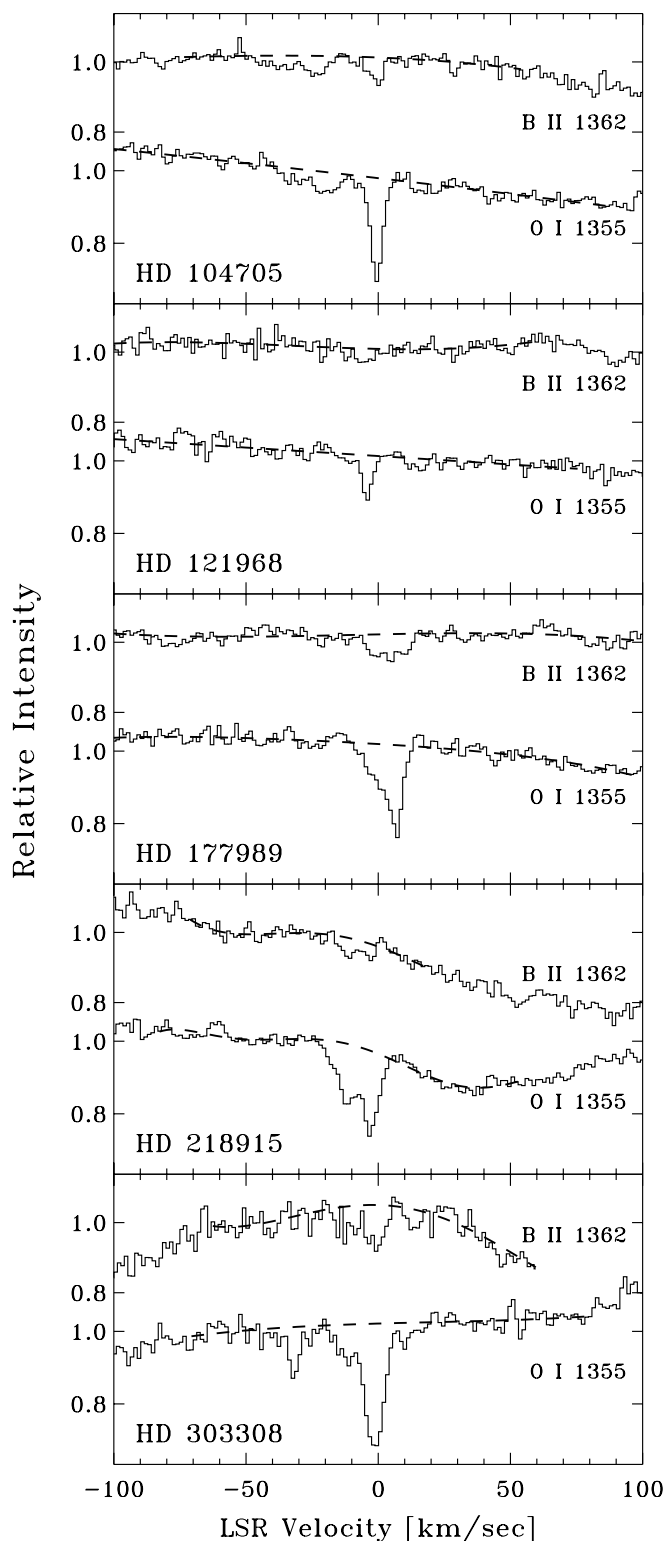


FIG. 1.—STIS absorption line spectra of B II  $\lambda 1362$  and O I  $\lambda 1355$  for five extended sight lines ( $d_* \gtrsim 2.5$  kpc) through the Milky Way. Our fits to the local stellar continua are shown by dashed lines. The velocity ranges over which we have integrated these spectra are given in Table 1.

GHRS measurements. The continua were estimated using low-order Legendre polynomial fits to regions free of interstellar lines, and our  $1\sigma$  error estimates include continuum placement uncertainties and the effects of 2% zero-point

TABLE 1  
EQUIVALENT WIDTH MEASUREMENTS

STAR	$W_\lambda^a$ (mÅ)		$(v_-, v_+)^b$	S/N <sup>c</sup>	
	O I $\lambda 1355$	B II $\lambda 1362$		O I	B II
STIS					
HD 104705.....	$11.8 \pm 0.8$	$5.3 \pm 1.2$	-48, +7	80	60
HD 121968.....	$3.0 \pm 0.5$	$1.8 \pm 0.6$	-12, +10	55	50
HD 177989.....	$10.4 \pm 0.5$	$4.8 \pm 0.4$	-12, +14	70	65
HD 218915.....	$14.3 \pm 0.9$	$2.3 \pm 0.6$	-17, +2	60	70
HD 303308.....	$18.4 \pm 1.5$	$8.0 \pm 1.6$	-20, +21	45	40
GHRS					
$\alpha$ Sco B.....	$11.4 \pm 0.8$	$1.6 \pm 0.5$	-5, +8	35	35
$\zeta$ Oph.....	$7.3 \pm 0.8^d$	$0.79 \pm 0.17$	-21, +7	56	370

<sup>a</sup> Measured equivalent width and  $1\sigma$  uncertainties.

<sup>b</sup> The range in  $v_{\text{LSR}}$  over which the absorption profiles were integrated.

<sup>c</sup> Empirically estimated signal-to-noise ratios for continuum regions near the O I and B II absorption lines, respectively.

<sup>d</sup> The O I  $\lambda 1355$  measurement for  $\zeta$  Oph is from Savage, Cardelli, & Sofia 1992 and represents the sum of their components A and B.

uncertainties for both spectrographs (Sembach & Savage 1992).

Federman et al. (1993) and Lambert et al. (1998) have studied the B II absorption along the  $\zeta$  Oph sight line using the GHRS with discrepant results. Federman et al. (1993) derive  $W_\lambda = 1.78 \pm 0.29$  mÅ using the G160M grating, while Lambert et al. (1998) derive  $W_\lambda = 0.6 \pm 0.2$  mÅ using the Ech-A grating. Given the differences in these studies, we have reanalyzed both GHRS data sets. We derive an equivalent width using the Ech-A of  $W_\lambda = 0.79 \pm 0.17$  mÅ, within  $1\sigma$  of the Lambert et al. result. We do not find clear evidence for B II absorption in the small science aperture G160M grating data to a  $3\sigma$  limiting equivalent width of  $W_\lambda < 1.3$  mÅ, consistent with our Ech-A results. However, the continuum placement uncertainties are large in this region of the spectrum when using the intermediate-resolution G160M grating. Alternative continuum placements could push this limiting equivalent width as high as 2.1 mÅ. We believe that the Ech-A results are the most reliable for this sight line, and we adopt  $W_\lambda = 0.79 \pm 0.17$  mÅ for the B II absorption toward  $\zeta$  Oph.

The sight line toward  $\alpha$  Sco B also deserves comment. The sight line to this star passes through the stellar wind of the M1.5 Ib primary (Antares), which lies  $2''.9$  from the  $\alpha$  Sco B sight line (van der Hucht, Bernat, & Kondo 1980; Bernat 1982; Cardelli 1984). It is therefore possible that the absorption lines in the spectra of  $\alpha$  Sco B probe the wind of the primary star. We do not believe that the O I and B II absorption seen in the archival GHRS spectra are caused by the stellar wind. These species show two blends of material centered at  $v_{\text{LSR}} = -4.1$  and  $+3.5$  km s<sup>-1</sup>. Material associated with the wind is centered near  $v_{\text{LSR}} = -18$  km s<sup>-1</sup> (van der Hucht et al. 1980). The archival GHRS data set contains good observations of lines that trace only the outflowing stellar wind, notably Ti II, Ti II\*, Ti II\*\*, and S I\*\*. These lines are clearly shifted with respect to the O I and B II absorption. They are centered near  $v_{\text{LSR}} = -18$  km s<sup>-1</sup>, often with wings extending toward more negative velocities. There is no evidence for wind material at the velocities of the O I and B II absorption. Therefore, we believe that the absorption-line measurements presented in Table 1 trace

the ISM in this direction rather than the stellar wind of Antares.<sup>4</sup>

### 3. RESULTS AND DISCUSSION

Table 2 gives the derived column densities of O I and B II for the stars listed in Table 1. Also given are the total hydrogen column densities and the normalized relative gas-phase abundances,  $[B/O]$ ,<sup>5</sup> for these sight lines. We also compile all measurements of interstellar B II using *HST* data from the literature (with references given in the table).

The new O I and B II column densities were derived by integrating the apparent optical depth profiles (Savage & Sembach 1991) of each line. In a few cases we have deemed it necessary to apply moderate saturation corrections to the O I column densities. We have tested for saturation problems and derived the necessary corrections by applying a single-component curve of growth to the measured O I equivalent widths (Table 1), adopting  $b$  values derived from a curve-of-growth fit to several C I lines for each sight line. The O I absorption is dominated by narrow components that are also strong in species that trace dense clouds, such as C I, S I, Cl I, and CO. While C I and O I need not be coexistent, the empirical association of C I and O I absorption, particularly in the components where the saturation is likely to be greatest, gives us confidence that C I saturation effects provide a suitable means for understanding the O I saturation along these sight lines. The O I apparent column densities we obtained for four of the sight lines from Table 1

<sup>4</sup> We also note that the column density of O I derived below is comparable to that of other stars in this region of sky with similar distances (Meyer et al. 1998).

<sup>5</sup> We define  $[B/O] \equiv \log N(B \text{ II})/N(O \text{ I}) - \log (B/O)_{\odot}$  and assume a meteoritic abundance of  $\log (B/O)_{\odot} = -5.99$  (Anders & Grevesse 1989).

required moderate saturation corrections of  $+0.06$  to  $+0.08$  dex based on the curve-of-growth fits, and these have been noted in Table 2.

Figure 2 shows the sight-line-integrated gas-phase abundances  $[B/O]$  as a function of average line-of-sight hydrogen densities,  $\langle n_H \rangle$ ,<sup>6</sup> for the 11 sight lines from Table 2. Where no H<sub>2</sub> column density measurements exist, we adopt a generous  $+0.25$  dex uncertainty in the total hydrogen column,  $N(H)$ , to account for the unknown contribution from molecular material. The bottom panel of Figure 2 shows  $[O/H]$  versus  $\langle n_H \rangle$  for the same sight lines. The dashed line shows the average value of  $[O/H] (= -0.34 \pm 0.02)$  from the sight lines studied by Meyer et al. (1998), several of which are included in this work.<sup>7</sup>

Figure 2 shows a clear trend of decreasing  $[B/O]$  abundance with increasing  $\langle n_H \rangle$ . Such a trend is often observed for species incorporated into interstellar dust grains (cf. Jenkins 1987). The general decrease in gas-phase abundance with increasing  $\langle n_H \rangle$  reflects the mixture of cold and warm diffuse clouds along the line of sight (Jenkins, Savage, & Spitzer 1986), where the cold clouds exhibit a greater incorporation of elements into interstellar grains.

All of the STIS targets in Table 2 have distances of  $d_* > 1000$  pc, while the GHRs targets are all at  $d_* < 500$  pc. It is conceivable that the gas being probed by the STIS data is also significantly more distant than that being probed by the GHRs data. In this case, some of the behavior seen in

<sup>6</sup> Defined  $\langle n_H \rangle \equiv N(H)/d_*$ , where  $d_*$  is the distance to the star from Table 2.

<sup>7</sup> We adopt the O I  $f$ -value suggested by D. C. Morton (2000, in preparation), which implies a  $+0.03$  dex correction to the O I column densities in Meyer et al. (1998).

TABLE 2  
STIS AND GHRs INTERSTELLAR BORON ABUNDANCE MEASUREMENTS

Star	ID <sup>a</sup>	$l^b$	$b^b$	$d_*^c$ (pc)	$\log N(O \text{ I})^d$	$\log N(B \text{ II})^d$	$\log N(H)^e$	$[B/O]^f$	Reference
HD 104705.....	1	297.4	-0.3	3900	$17.83 \pm 0.03$	$11.53^{+0.09}_{-0.11}$	$21.11^{+0.25}_{-0.07}$	$-0.31^{+0.10}_{-0.12}$	1
HD 121968.....	2	334.0	+55.8	3600	$17.21 \pm 0.07$	$11.06^{+0.12}_{-0.18}$	$20.71^{+0.25}_{-0.08}$	$-0.17^{+0.14}_{-0.19}$	1
HD 177989.....	3	17.8	-11.9	4900	$17.84 \pm 0.03^g$	$11.48^{+0.04}_{-0.04}$	$20.95^{+0.25}_{-0.09}$	$-0.37^{+0.05}_{-0.05}$	1
HD 218915.....	4	108.1	-6.9	3600	$17.97 \pm 0.03^g$	$11.16^{+0.10}_{-0.13}$	$21.30^{+0.25}_{-0.08}$	$-0.82^{+0.10}_{-0.13}$	1
HD 303308.....	5	287.6	-0.6	2600	$18.10 \pm 0.04^g$	$11.71^{+0.08}_{-0.10}$	$21.45^{+0.25}_{-0.09}$	$-0.40^{+0.09}_{-0.11}$	1
$\zeta$ Oph.....	6	6.3	+23.6	$140^{+15}_{-12}$	$17.68 \pm 0.05$	$10.69^{+0.09}_{-0.11}$	$21.15^{+0.03}_{-0.03}$	$-1.00^{+0.10}_{-0.12}$	1, 2
$\alpha$ Sco B.....	7	352.0	+15.1	158	$17.91 \pm 0.03^g$	$11.01^{+0.12}_{-0.16}$	$21.43^{+0.25}_{-0.10}$	$-0.91^{+0.12}_{-0.16}$	1
$\delta$ Sco.....	8	350.1	+22.5	$123^{+15}_{-12}$	$17.74 \pm 0.06^h$	$10.93^{+0.09}_{-0.11}$	$21.08^{+0.07}_{-0.07}$	$-0.82^{+0.11}_{-0.13}$	3, 4
$\kappa$ Ori.....	9	214.5	-18.5	$220^{+50}_{-32}$	$17.03 \pm 0.04$	$10.63^{+0.11}_{-0.15}$	$20.53^{+0.04}_{-0.04}$	$-0.41^{+0.12}_{-0.15}$	3, 4
$\lambda$ Ori.....	10	195.1	-12.0	$320^{+90}_{-60}$	$17.33 \pm 0.06$	$10.79^{+0.11}_{-0.15}$	$20.81^{+0.07}_{-0.07}$	$-0.55^{+0.13}_{-0.16}$	3, 5
$\iota$ Ori.....	11	209.5	-19.6	$410^{+180}_{-100}$	$16.76 \pm 0.07$	$< 10.30$	$20.18^{+0.05}_{-0.05}$	$< -0.47$	3, 5

<sup>a</sup> Identification number designating the observed stars in Figure 2.

<sup>b</sup> Galactic coordinates for the observed stars.

<sup>c</sup> Distances to the observed stars. Where available, we have used *Hipparcos* (Perryman et al. 1997) distances (those distances with error bars). Otherwise we have adopted distances from Diplas & Savage 1994.

<sup>d</sup> Logarithmic column densities and  $1 \sigma$  error estimates (in units atoms  $\text{cm}^{-2}$ ) for O I and B II derived by integrating the apparent column density profiles. We adopt oscillator strengths from D. C. Morton 2000 (in preparation):  $f(O \text{ I } 1355) = 1.16 \times 10^{-6}$  and  $f(B \text{ II } 1362) = 0.998$ .

<sup>e</sup> Total logarithmic hydrogen column density  $N(H) = N(H \text{ I}) + 2N(H_2)$ . For many sight lines, no H<sub>2</sub> column densities are available, and we have adopted H I column densities from Diplas & Savage 1994 with an upper error bar of  $+0.25$  dex. All other measurements are a weighted mean of the Bohlin, Savage, & Drake 1978 and Diplas & Savage 1994 H I column densities combined with the Savage et al. 1977 H<sub>2</sub> column densities.

<sup>f</sup> Relative logarithmic abundance of boron to oxygen, referenced to the relative solar system values such that  $[B/O] \equiv \log N(B \text{ II})/N(O \text{ I}) - \log (B/O)_{\odot}$ , where  $\log (B/O)_{\odot} = -5.99$  (Anders & Grevesse 1989).

<sup>g</sup> Small saturation corrections have been made to the original apparent column densities based upon the C I curve of growth for each sight line. The applied corrections are (in dex)  $+0.06$ ,  $+0.06$ ,  $+0.06$ , and  $+0.08$  for HD 177989, HD 218915, HD 303308, and  $\alpha$  Sco B, respectively.

<sup>h</sup> The O I column density for the  $\delta$  Sco sight line is derived from *Copernicus* observations of the 1355 Å transition (see Meyer et al. 1998).

REFERENCES.—For O I and B II column densities: (1) This work; (2) Savage et al. 1992; (3) Meyer et al. 1998; (4) Lambert et al. 1998; (5) Jura et al. 1996.

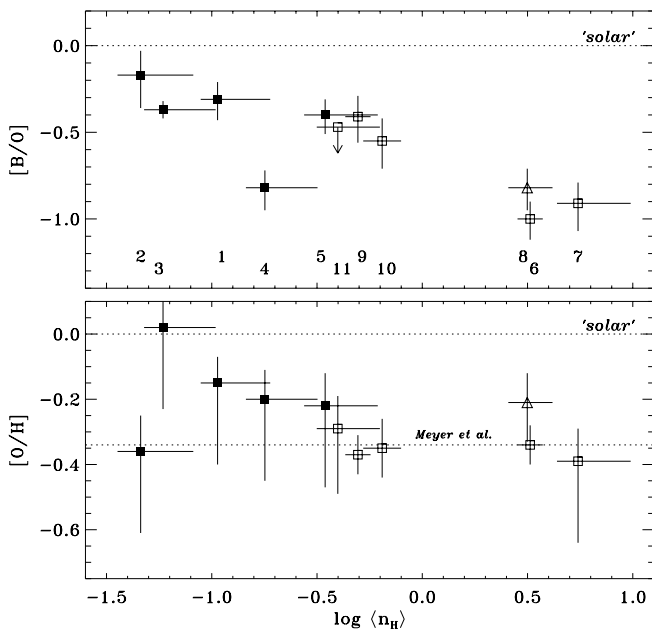


FIG. 2.—Measurements of sight-line-integrated  $[B/O]$  (top) and  $[O/H]$  (bottom) abundances as a function of the average sight-line hydrogen density,  $\langle n_{\text{H}} \rangle [\equiv N(\text{H})/d_*]$ . The numbers in the top panel identify each sight line according to the ID in Table 2. The filled squares show new measurements derived from STIS observations of O I and B II, and the open squares show GHRs measurements taken from the literature or from an analysis of data in the *HST* archive. The open triangle shows a GHRs B II measurement coupled with a *Copernicus* O I measurement. The dashed line in the bottom panel shows the average  $[O/H]$  value from the measurements of Meyer et al. (1998) after correcting for our adopted O I  $f$ -value. The  $[O/H]$  measurements with the 0.25 dex downward error bars represent sight lines for which  $N(\text{H}_2)$  has not been measured, and  $N(\text{H})$  is assumed to be  $N(\text{H I})$ .

Figure 2 could be caused by abundance gradients. There are several reasons to believe that this is not the case. First, of the 11 stars in our sample (Table 2), eight have galactocentric distances between 7.5 and 9.5 kpc, i.e., they lie within 1 kpc of the solar circle. Within this 2 kpc range in galactocentric distance, the  $[B/O]$  abundance varies from  $-0.31^{+0.10}_{-0.12}$  to  $-1.00^{+0.10}_{-0.12}$ , i.e., the abundance varies by a factor of 5. Thus, most of the trend seen in Figure 2 occurs within 1 kpc galactocentric distance of the solar circle and cannot be caused by large-scale abundance gradients.

Second, there is evidence that the absorption along all the sight lines actually arises within the first 1–2 kpc. Most of the absorption seen in Figure 1 is at velocities that are consistent with nearby material, and given that typical cloud-to-cloud velocity dispersions are of the order of  $\sigma \sim 8 \text{ km s}^{-1}$  (Sembach & Danks 1994), most of the gas is likely very local. For example, although the extended STIS sight lines toward HD 177989 and HD 218915 pass over known spiral arms with prominent absorption in other species (e.g., Mg II, Mn II, Ni II, Cu II, and Ge II), there is no evidence for any absorption in the weak O I and B II lines from those distant structures. The nearest arms probed along these sight lines are the Perseus arm seen toward HD 218915 at a distance of  $\sim 2.5$  kpc and the Sagittarius arm toward HD 177989, which is likely at a distance of  $\sim 1.8$  kpc. The Perseus and Sagittarius arms are seen in absorption in other species at  $v_{\text{LSR}} \approx -45$  and  $+18 \text{ km s}^{-1}$  toward HD 218915 and HD 177989, respectively.

The relatively local origin of the gas toward HD 218915 may explain why it does not fit well the general trend with average sight line density seen in Figure 2 (point 4 in this figure). One would prefer to use a more physically meaningful measure of physical conditions, such as the fraction of hydrogen in molecular form,  $f(\text{H}_2) \equiv 2N(\text{H}_2)/N(\text{H})$ . Figure 3 shows the  $[B/O]$  abundances versus  $f(\text{H}_2)$  for those sight lines with  $N(\text{H}_2)$  measurements. This diagram is sparsely populated, but there seems to be a slight trend of increasing  $[B/O]$  abundance with decreasing  $f(\text{H}_2)$ . For this diagram to be truly useful, however, more  $N(\text{H}_2)$  measurements are needed. The *Far Ultraviolet Spectroscopic Explorer* will soon provide molecular hydrogen column densities for a large number of sight lines toward distant stars, making it possible to fill in the missing points in Figure 3.

The trend seen in Figure 2, and the fact that the more distant stars studied by STIS show higher  $[B/O]$  abundances, is likely caused by the heights of these stars above the plane of the Galaxy. Because the stars studied by STIS are more distant, they generally lie at larger distances from the Galactic plane than do the stars studied by the GHRs. Thus, the sight lines probed by our STIS measurements probe lower density regions, on average, than the sight lines probed by the GHRs measurements. The well-documented trend of higher gas-phase abundances of most elements in lower density regions suggests that we should expect the segregation of STIS and GHRs measurements observed in Figure 2.

While the average sight-line  $[B/O]$  values show a clear trend with  $\langle n_{\text{H}} \rangle$ , an imperfect measure of sight-line properties, there is also evidence within the observed line profiles for variation of  $[B/O]$  with the physical properties of the absorbing material. Several of the sight lines displayed in Figure 1 show evidence for dense clouds with lower B/O ratios than warm clouds along the same line of sight, in qualitative agreement with the Jenkins et al. (1986) model of integrated sight-line properties. Figure 4 shows the apparent column density (Savage & Sembach 1991), or  $N_a(v)$ , profile of B II  $\lambda 1362$  toward HD 104705 with the corresponding  $N_a(v)$  profiles of O I  $\lambda 1355$  and Ga II  $\lambda 1414$ . This sight line exhibits a narrow, cold component centered at  $v_{\text{LSR}} = 0 \text{ km s}^{-1}$ , which is prominent in species such as O I, S I, Cl I, and CO, as well as a blend of warmer components

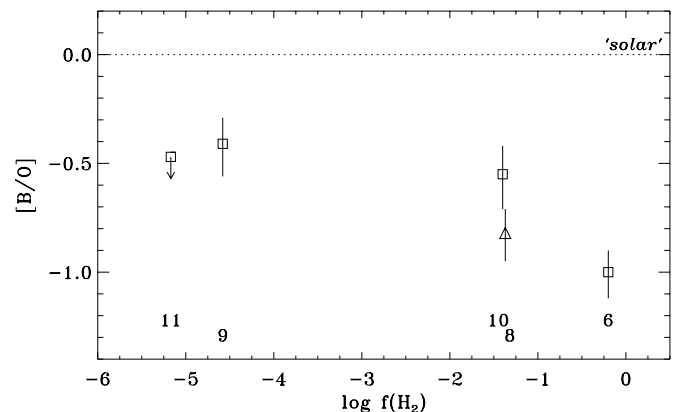


FIG. 3.—Measurements of sight-line-integrated  $[B/O]$  abundances as a function of logarithmic fraction of hydrogen in molecular form,  $f(\text{H}_2) \equiv 2N(\text{H}_2)/N(\text{H})$ , for the sight lines with measured  $N(\text{H}_2)$ . The sight-line numbering and symbol definitions are the same as in Fig. 2.

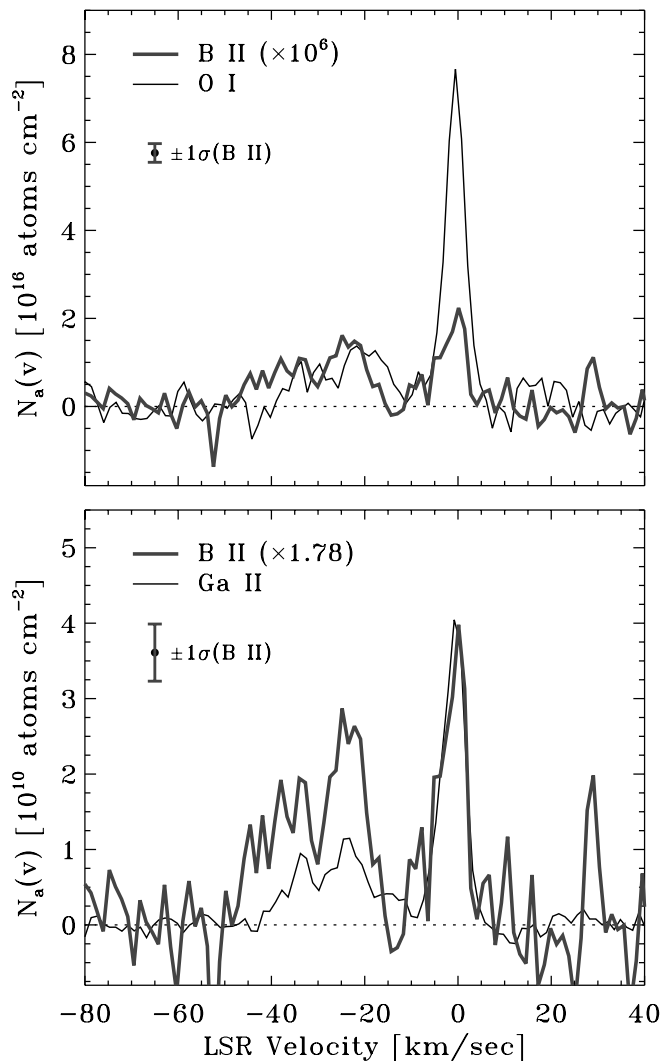


FIG. 4.—Apparent column density, or  $N_a(v)$ , profile for B II  $\lambda 1362$  plotted with those of O I  $\lambda 1355$  (top), and Ga II  $\lambda 1414$  (bottom) for the line of sight to HD 104705. The B II profiles have been scaled by the appropriate solar system abundances (Anders & Grevesse 1989) of O/B ( $10^6$ ) and Ga/B (1.78). The narrow component near  $v_{\text{LSR}} = 0 \text{ km s}^{-1}$  shows subsolar B/O ratios, while the warm gas between  $v_{\text{LSR}} = -40$  and  $-15 \text{ km s}^{-1}$  exhibits almost solar B/O. The narrow component also shows solar B/Ga abundance, while the negative velocity material has supersolar relative B/Ga abundances. This behavior suggests that boron is incorporated into dust and is more readily stripped from the grains than gallium. A typical  $\pm 1\sigma$  error bar is shown for the B II profile.

between  $v_{\text{LSR}} = -40$  and  $-10 \text{ km s}^{-1}$ . Figure 4 shows that the B/O ratio changes between these two regions. The integrated abundances in these two components are significantly different:  $[\text{B}/\text{O}] = -0.57^{+0.12}_{-0.16}$  for the component centered at  $v_{\text{LSR}} = 0 \text{ km s}^{-1}$ , and  $[\text{B}/\text{O}] = +0.08^{+0.13}_{-0.17}$  for the blend of warm components at negative velocities. This sight line exhibits variations in  $[\text{B}/\text{O}]$  that are coupled to real changes in the physical properties of the observed components.

The dependence of  $[\text{B}/\text{O}]$  on  $\langle n_{\text{H}} \rangle$  could potentially be caused by other effects, including true abundance variations (gas + dust) and differential ionization (e.g., Sembach et al. 2000). Boron may be particularly sensitive to the latter effect, since its second ionization potential is high (25.15 eV,

similar to that of C II). While the effects of differential ionization may modify the component-to-component B/O ratios, they are likely not large enough (perhaps  $\lesssim 0.1$  dex) to cause the 0.8 dex range of  $[\text{B}/\text{O}]$  seen in Figure 2.

We believe that the incorporation of boron into grains is dominant among the possible effects leading to the trend seen in Figure 2. It is reasonable to expect that boron should be incorporated into dust. It has a condensation temperature (910–964 K; Zhai 1995; Lauretta & Lodders 1996) similar to those of gallium and copper, and is in the same group of the periodic table as aluminum and gallium, all of which are known to be significantly incorporated into interstellar dust (Hobbs et al. 1993; Savage & Sembach 1996).

The cold cloud toward HD 104705 (Fig. 4) shows a solar B/Ga ratio, although the blend of warm components exhibits supersolar B/Ga ratios. If the abundance variations between these regions are caused by the destruction of dust (see Savage & Sembach 1996), then boron is more readily stripped from grains than is gallium.

The gas-phase abundance measurements of boron in Table 2 yield no firm information on the solid-phase abundance of boron. We derive a lower limit to the present-day total (gas + dust) interstellar boron abundance of  $\text{B}/\text{H} \gtrsim (2.5 \pm 0.9) \times 10^{-10}$  (using the measured  $[\text{B}/\text{O}]$  toward HD 121968 and assuming  $[\text{O}/\text{H}] = -0.34 \pm 0.02$  from Meyer et al. 1998, corrected for the D. C. Morton 2000, in preparation, O I  $f$ -value). The interstellar B/H is lower than the meteoritic abundances  $[\text{B}/\text{H}] = (7.6 \pm 0.7) \times 10^{-10}$ ; Anders & Grevesse 1989] and non-LTE abundances for stars of solar-like metallicity ( $\text{B}/\text{H} = 5 \times 10^{-10}$ ; see discussion in Lambert et al. 1998).

The probable incorporation of boron into interstellar dust makes it difficult to use the measured gas-phase interstellar boron abundance to study the influence of spallation on the chemical evolution of the light elements. Another probe of spallation-induced chemical evolution is the  $^{11}\text{B}/^{10}\text{B}$  isotope ratio (cf. Lambert et al. 1998), and some of the sight lines presented here might allow accurate measurements of this ratio with higher resolution or signal to noise. In fact, the sight line toward HD 104705 seems to show a high  $^{11}\text{B}/^{10}\text{B}$  ratio; the red wing of the B II profile is very similar to that of the Ga II profile. However, the relative component structure seen in the  $N_a(v)$  profiles of B II toward HD 104705, HD 177989, and HD 218915 are significantly different from all of the other ionic species covered by our observations, including Ga II, Cu II, and Ge II. The depletion and/or ionization characteristics of B II are dissimilar to these species, perhaps making it inappropriate to use them as templates for B II when studying the  $^{11}\text{B}/^{10}\text{B}$  ratio along complicated sight lines.

#### 4. SUMMARY

We have presented new and archival observations of the gas-phase abundance of boron in the diffuse interstellar medium using STIS and GHRS. From our analysis of these high-quality absorption-line data, and measurements from the literature, we have concluded the following.

1. The gas-phase abundance of  $[\text{B}/\text{O}]$  in the ISM is anticorrelated with the average density of hydrogen along the sight line being probed, as well as the fraction of hydrogen seen in molecular form along a sight line. Along individual sight lines, we also find a significantly higher gas-phase

[B/O] abundance in warm than in cold diffuse clouds. The evidence strongly suggests that boron is incorporated into dust grains in the diffuse ISM.

2. The relative component-to-component strengths in the observed B II profiles are significantly different from those of any other observed species, including Ga II, Cu II, and Ge II. The depletion and/or ionization characteristics of B II are different from those of other species. Although Ga II, Cu II, and Ge II are sometimes used as templates for modeling the B II absorption, the differences seen in our data suggest that it may be inappropriate to assume that they

trace the B II profile when deriving the  $^{11}\text{B}/^{10}\text{B}$  ratio along complicated sight lines.

3. We derive a lower limit to the present-day total (gas + dust) B/H abundance of  $\text{B}/\text{H} \gtrsim (2.5 \pm 0.9) \times 10^{-10}$ .

We thank S. Federman for suggestions on this work. This work was supported by NASA through grants GO-0720.01-96A and GO-0720.02-96A from the Space Telescope Science Institute, which is operated by the Association of Universities for Research in Astronomy, Inc., under NASA contract NASS-26555.

#### REFERENCES

- Anders, E., & Grevesse, N. 1989, *Geochim. Cosmochim. Acta*, 53, 197  
 Bernat, A. P. 1982, *ApJ*, 252, 644  
 Bohlin, R. C., Savage, B. D., & Drake, J. F. 1978, *ApJ*, 224, 132  
 Cardelli, J. A. 1984, *AJ*, 89, 1825  
 Cunha, K., Lambert, D. L., Lemke, M., Gies, D. R., & Roberts, L. C. 1997, *ApJ*, 478, 211  
 Diplas, A., & Savage, B. D. 1994, *ApJS*, 93, 211  
 Duncan, D. K., et al. 1997, *ApJ*, 488, 338  
 Edvardsson, B., Gustafsson, B., Johansson, S. G., Kiselman, D., Lambert, D. L., Nissen, P. E., & Gilmore, G. 1994, *A&A*, 290, 176  
 Federman, S. R., Lambert, D. L., Cardelli, J. A., & Sheffer, Y. 1996, *Nature*, 381, 764  
 Gies, D. R., & Lambert, D. L. 1992, *ApJ*, 387, 673  
 Hobbs, L. M., Welty, D. E., Morton, D. C., Spitzer, L., & York, D. G. 1993, *ApJ*, 411, 750  
 Howk, J. C., Savage, B. D., & Fabian, D. 1999, *ApJ*, 525, 253  
 Howk, J. C., & Sembach, K. R. 2000, *AJ*, 119, 2481  
 Jenkins, E. B. 1987, in *Interstellar Processes*, ed. D. J. Hollenbach & H. A. Thronson, Jr. (Dordrecht: Reidel), 533  
 Jenkins, E. B., Savage, B. D., & Spitzer, L. 1986, *ApJ*, 301, 355  
 Jura, M., Meyer, D. M., Hawkins, I., & Cardelli, J. A. 1996, *ApJ*, 456, 598  
 Kilian-Montenbruck, J., Gehren, T., & Nissen, P. E. 1994, *A&A*, 291, 757  
 Lambert, D. L., Sheffer, Y., Federman, S. R., Cardelli, J. A., Sofia, U. J., & Knauth, D. C. 1998, *ApJ*, 494, 614  
 Lauretta, D. S., & Lodders, K. 1996, *Meteor. Planet. Sci.*, 31, A77  
 Meneguzzi, M., Audouze, J., & Reeves, H. 1971, *A&A*, 15, 337  
 Meyer, D. M., Jura, M., & Cardelli, J. A. 1998, *ApJ*, 493, 222  
 Pagel, B. E. J. 1997, *Nucleosynthesis and Chemical Evolution of Galaxies* (Cambridge: Cambridge Univ. Press)  
 Peimbert, M., Torres-Peimbert, S., & Dufour, R. J. 1993, *ApJ*, 418, 760  
 Perryman, M. A. C., et al. 1997, *A&A*, 323, L49  
 Reeves, H., Fowler, W. A., & Hoyle, F. 1970, *Nature*, 226, 727  
 Savage, B. D., Bohlin, R. C., Drake, J. F., & Budich, W. 1977, *ApJ*, 216, 291  
 Savage, B. D., Cardelli, J. A., & Sofia, U. J. 1992, *ApJ*, 401, 706  
 Savage, B. D., & Sembach, K. R. 1991, *ApJ*, 379, 245  
 ———. 1996, *ARA&A*, 34, 279  
 Sembach, K. R., & Danks, A. C. 1994, *A&A*, 289, 539  
 Sembach, K. R., Howk, J. C., Ryans, R. S. I., & Keenan, F. P. 2000a, *ApJ*, 528, 310  
 Sembach, K. R., & Savage, B. D. 1992, *ApJS*, 83, 147  
 van der Hucht, K. A., Bernat, A. P., & Kondo, Y. 1980, *A&A*, 82, 14  
 Woosley, S. E., Hartmann, D. H., Hoffman, R. D., & Haxton, W. C. 1990, *ApJ*, 356, 272  
 Zhai, M. 1995, *Meteoritics*, 29, 607